Supplementary Information: Bound states in the continuum of higher-order topological insulators

Wladimir A. Benalcazar and Alexander Cerjan
Department of Physics, The Pennsylvania State University, University Park, Pennsylvania 16802, USA

In this document we characterize the topological phases of the pristine lattice with Bloch Hamiltonian in Eq. 1 of the Main Text, their topological invariants, and their associated Wannier centers. We then discuss the implementation of terms that once added to the Hamiltonian in Eq. 1 of the Main Text, break certain symmetries, possibly transforming the BICs into high-order topological resonances. Finally, we present plots of the energies of the system as a function of system size to conclude that the spread of higher-order topological resonances are not due to finite size effects in the simulations.

A. Irreducible representations of the energy bands of the lattice model

The Hamiltonian in Eq. 1 of the Main Text has C_{4v} symmetry, which is generated by the simultaneous presence of C_4 symmetry,

$$\hat{r}_4 h(k_x, k_y)\hat{r}_4^\dagger = h(k_y, -k_x), \tag{S1}$$

and reflection symmetry,

$$\hat{M}_x h(k_x, k_y)\hat{M}_x^\dagger = h(-k_x, k_y), \tag{S2}$$

both of which imply also C_2 symmetry as well as reflection symmetries along y -denoted M_y- and along the two diagonals -denoted M_{d1} and M_{d2}. The topology of the crystalline phases of this model can be diagnosed by looking at the representations that the states take at the high-symmetry points (HSPs) of the Brillouin zone. In particular, we are interested in the HSPs $\mathbf{\Gamma}$ and $\mathbf{M}$, which are invariant under the full group, C_{4v}, as well as the HSPs $\mathbf{\Gamma}$, $\mathbf{X}$, and $\mathbf{X}'$, which are invariant only under the little group C_{2v}. The representations that each of these bands take at these points is given in Table S1.

The irreducible representations in Table S1 have the character tables detailed in Table S2.

Notice that only the group C_{4v} has a two-dimensional irreducible representation, E. This is the representation of the bulk states at zero energy and which coexist with the topological corner BICs.

phase	bands	C_{4v}		C_{2v}		
		$\mathbf{\Gamma}$	$\mathbf{M}$	$\mathbf{\Gamma}$	$\mathbf{X}$	$\mathbf{X}'$
$\lvert t\rvert < 1$	1	B_2	A_1	a_2	b_1	b_2
	2,3	E	E	$b_1 + b_2$	$a_1 + a_2$	$a_1 + a_2$
	4	A_1	B_2	a_1	b_2	b_1
$\lvert t\rvert > 1$	1	B_2	B_2	a_2	a_2	a_2
	2,3	E	E	$b_1 + b_2$	$b_1 + b_2$	$b_1 + b_2$
	4	A_1	A_1	a_1	a_1	a_1

TABLE S1. Symmetry representations at the high symmetry points of the BZ in both topological ($|t| < 1$) and trivial ($|t| > 1$) phases. Irreducible representations (irreps) at $\mathbf{\Gamma}$ and $\mathbf{M}$ are for C_{4v} and irreps at $\mathbf{X}$ and $\mathbf{X}'$ are for C_{2v}. Irreps A_1, A_2, B_1, B_2, a_1, a_2, b_1, b_2 are one dimensional. Irrep E is two-dimensional.

irrep	I	C_2	$2C_4$	$2M_v$	$2M_d$
A_1	1	1	1	1	1
A_2	1	1	1	-1	-1
B_1	1	1	-1	1	-1
B_2	1	1	-1	-1	1
E	2	-2	0	0	0

irrep	I	C_2	M_x	M_y
a_1	1	1	1	1
a_2	1	1	-1	-1
b_1	1	-1	1	-1
b_2	1	-1	-1	1

TABLE S2. Character table for the C_{4v} (left) and C_{2v} (right) groups. The irreducible representations at the HSPs of the Brillouin zone for each energy band is shown in Table S1.

B. Trivial and topological phases of the model and their Wannier centers

In real space, the topology of the energy bands in the lattice of Fig. 1(a) in the Main Text determines the positions of their Wannier centers [1, 2]. Although the Block Hamiltonian in Eq. 1 in the Main Text has C_{4v} and chiral symmetries, C_4 or C_2 symmetries alone suffice to fix the positions of the Wannier centers to one of two disconnected maximal Wyckoff positions of the lattice: a 'trivial' Wannier center for $|t| > 1$, and a 'topological' one, for $|t| < 1$. These two phases are in different *atomic limits* [3]. The trivial atomic limit ($|t| > 1$) is described by Wannier centers that coincide with the centers of the unit cells [Fig. S1(a)], and the nontrivial atomic limit ($|t| < 1$) has Wannier centers at the corners of the unit cells [Fig. S1(b)]. In particular, when boundaries are open in both directions, the nontrivial atomic limit has a mismatch in the number of Wannier centers relative

to the number of unit cells [Fig. S1(b)] which results in a fractional density of states at corners [Fig. 1(c), lower panels].

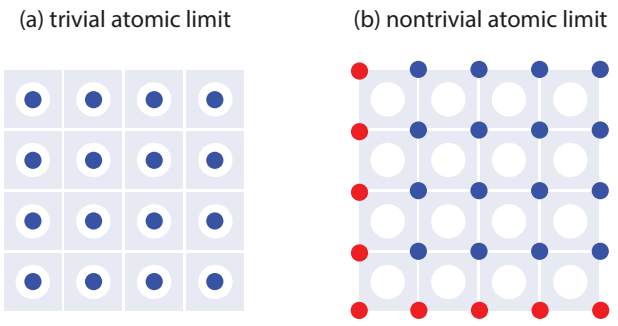

FIG. S1. Wannier center configuration for (a) the trivial phase, $|t| > 1$ and (b) the topological phase, $|t| < 1$ for all bands in the model of Eq. 1 of the Main Text. Gray squares are unit cells. Blue and red circles are the Wannier centers. White circles represent the centers of the unit cells. In (b), Wannier centers in red are in excess relative to those with closed boundaries, inducing filling anomalies that result in fractional density of states at corners.

These two configurations can be diagnosed from symmetry indicator topological invariants, which are derived from the symmetry representations that each of the bands take at the HSPs of the Brillouin zone. Table. S3 compiles the representations for C_2 and C_4 symmetries. From these representations, we can calculate the symmetry indicator invariants for all the bands defined as follows,

phase	bands	C_4		C_2		
		$\mathbf{\Gamma}$	$\mathbf{M}$	$\mathbf{\Gamma}$	$\mathbf{X}$	$\mathbf{X}'$
$\|t\| < 1$	1	-1	$+1$	$+1$	-1	-1
	2,3	$\pm i$	$\pm i$	$\{-1,-1\}$	$\{+1,+1\}$	$\{+1,+1\}$
	4	$+1$	-1	$+1$	-1	-1
$\|t\| > 1$	1	$+1$	$+1$	$+1$	$+1$	$+1$
	2,3	$\pm i$	$\pm i$	$\{-1,-1\}$	$\{-1,-1\}$	$\{-1,-1\}$
	4	$+1$	$+1$	$+1$	$+1$	$+1$

TABLE S3. Symmetry representations at the high symmetry points of the BZ in both topological ($|t| < 1$) and trivial ($|t| > 1$) phases. Irreducible representations (irreps) at $\mathbf{\Gamma}$ and $\mathbf{M}$ are for C_4 and irreps at $\mathbf{X}$ and $\mathbf{X}'$ are for C_2.

$$[\Pi_p] = \#\Pi_p - \#\Gamma_p, \tag{S3}$$

where $\#\Pi_p$ is the number of states in a particular band at high symmetry point $\mathbf{\Pi} = \mathbf{X}$, $\mathbf{Y}$, and $\mathbf{M}$, with eigenvalue $\Pi_p = e^{2\pi p/n}$, for $p = 0 \ldots n-1$, and $n = 2, 4$ for $C_{n=2,4}$ symmetry, respectively.

From these invariants it is possible to determine the dipole moments of the bands according to the following expressions,

phase	bands	Invariants			$Q^{(4)}_{corner}$
		$[X_1]$	$[M_1]$	$[M_2]$	
$\|t\| < 1$	1	-1	$+1$	0	$\frac{1}{4}$
	2,3	2	0	0	$\frac{1}{2}$
	4	-1	-1	0	$\frac{1}{4}$
$\|t\| > 1$	1	0	0	0	0
	2,3	0	0	0	0
	4	0	0	0	0

TABLE S4. C_4 symmetry indicator invariants and filling anomaly topological indices in both topological ($|t| < 1$) and trivial ($|t| > 1$) phases.

phase	bands	Invariants			$Q^{(2)}_{corner}$
		$[X_1]$	$[Y_1]$	$[M_1]$	
$\|t\| < 1$	1	-1	-1	0	$\frac{1}{2}$
	2,3	2	2	0	0
	4	-1	-1	0	$\frac{1}{2}$
$\|t\| > 1$	1	0	0	0	0
	2,3	0	0	0	0
	4	0	0	0	0

TABLE S5. C_2 symmetry indicator invariants and filling anomaly topological indices in both topological ($|t| < 1$) and trivial ($|t| > 1$) phases.

$$\mathbf{P}^{(4)} = \frac{1}{2}[X_1^{(2)}](\mathbf{a_1} + \mathbf{a_2}) \tag{S4}$$

when protected by C_4 symmetry and

$$\mathbf{P}^{(2)} = \frac{1}{2}([Y_1^{(2)}] + [M_1^{(2)}])\mathbf{a_1} + \frac{1}{2}([X_1^{(2)}] + [M_1^{(2)}])\mathbf{a_2} \tag{S5}$$

when protected by C_2 symmetry [4]. In the topological phase, $\mathbf{P} = (\frac{e}{2}, \frac{e}{2})$. With open boundaries, these moments generate an *edge-induced filling anomaly* [4], an excess in the number of states relative to those with no boundaries. In addition, this configuration has a (nominal) corner-induced filling anomaly [4]: an extra excess or depletion of states caused only in the presence of corners, which can be calculated via the following topological indices,

$$Q^{(4)}_{corner} = \frac{1}{4}([X_1] + 2[M_1] + 3[M_2]) \tag{S6}$$

when protected by C_4 symmetry and

$$Q^{(2)}_{corner} = \frac{1}{4}(-[X_1] - [Y_1] + [M_1]) \tag{S7}$$

when protected by C_2 symmetry.

The filling anomaly causes existence of corner-localized states that constitute topological BICs (if additionally C_{4v} and chiral symmetries are preserved) or topological resonances (if either C_{4v} or chiral are broken). We emphasize that not all lattices with $\mathbf{P} = (\frac{e}{2}, \frac{e}{2})$ have a corner-induced filling anomaly. A case in point is the lattice in Fig. 2(e) in Ref. 4.

The symmetry indicator invariants and their topological indices for polarization and corner filling anomalies for the bands in our model are shown in Table S4 and S5.

C. Constraints on the energy spectrum due to chiral symmetry

Consider the energy eigenstate $|u\rangle$ with energy ϵ, such that

$$h\,|u\rangle = \epsilon\,|u\rangle\,. \tag{S8}$$

If the Hamiltonian h has chiral symmetry, $\{h, \Pi\} = 0$, then the state $\Pi\,|u\rangle$ is an energy eigenstate of h with energy $-\epsilon$,

$$h\Pi\,|u\rangle = -\Pi h\,|u\rangle = -\epsilon\Pi\,|u\rangle \tag{S9}$$

Thus, the energies in a system with chiral symmetry come in pairs $(\epsilon, -\epsilon)$, and their states are related by the chiral operator Π. From this, it follows that states with $\epsilon = 0$ are either eigenstates of Π, in which case have support only in one sublattice, or come in pairs $(|u\rangle\,, \Pi\,|u\rangle)$. In the Hamiltonian of Eq. 1 in the Main Text, examples of the first case are the individual zero energy corner states, while an example of the second case is the subspace of bulk states at zero energy.

D. Implementing the symmetry-breaking perturbations

To generate the results in Fig. 4 of the Main Text, additional hopping terms where added to the Hamiltonian of Eq. 1 in the Main Text. The overall Hamiltonian *before introducing losses in the system, Eq. 2 in the Main Text*, is

$$h_T(\mathbf{k}) = h(\mathbf{k}) + \Delta_p h_p(\mathbf{k}), \tag{S10}$$

where Δ_p is the overall strength of the perturbation and

$$\begin{aligned} h_p(\mathbf{k}) =& T_{x1}\cos k_x + T_{x2}\sin k_x + T_{y1}\cos k_y + T_{y2}\sin k_y \\ &+ T_1\cos k_x \sin k_y + T_2 \sin k_x \cos k_y \end{aligned} \tag{S11}$$

is the Hamiltonian of the additional perturbation, which amounts to hopping terms up to next nearest neighbor unit cells. The T matrices are all 4×4 random Hermitian matrices in which each entry has a complex value with a uniform distribution in the range $[0, 1]$. In addition to obeying Hermicity, the T matrices are subject to certain constraints imposed by the symmetries we are interested in preserving. In what follows we detail examples of the constraints on the T matrices used for the preservation of certain symmetries:

1. *For chiral symmetry*

Under chiral symmetry, $\Pi h(\mathbf{k})\Pi = -h(\mathbf{k})$, all T matrices must obey

$$\{T, \Pi\} = 0. \tag{S12}$$

2. *For C_4 symmetry*

Let us first focus on the nearest neighbor T matrices. To first satisfy C_2 symmetry, $\hat{r}_2 h(k_x, k_y)\hat{r}_2^\dagger = h(-k_x, -k_y)$, we require

$$[T_{x1}, \hat{r}_2] = 0, \quad \{T_{x2}, \hat{r}_2\} = 0. \tag{S13}$$

Now, to satisfy C_4 symmetry, $\hat{r}_4 h(k_x, k_y)\hat{r}_4^\dagger = h(k_y, -k_x)$, we additionally require

$$T_{y1} = \hat{r}_4 T_{x1}\hat{r}_4^\dagger, \quad T_{y2} = -\hat{r}_4 T_{x2}\hat{r}_4^\dagger. \tag{S14}$$

The two next nearest neighbor T matrices are odd under C_2 symmetry. Take first T_1 to obey

$$\{T_1, \hat{r}_2\} = 0, \tag{S15}$$

and then determine T_2 via the constraint due to C_4 symmetry,

$$T_2 = -\hat{r}_4 T_2 \hat{r}_4^\dagger. \tag{S16}$$

3. *For reflection symmetry*

Under reflection symmetry along x, $\hat{M}_x h(k_x, k_y)\hat{M}_x^\dagger = h(-k_x, k_y)$, four T matrices are even under M_x and two are odd,

$$\begin{aligned} [T_{x1}, \hat{M}_x] = 0 \quad &, [T_{y1}, \hat{M}_x] = 0, \\ [T_{y2}, \hat{M}_x] = 0, \quad &[T_1, \hat{M}_x] = 0, \\ \{T_{x2}, \hat{M}_x\} = 0, \quad &\{T_2, \hat{M}_x\} = 0. \end{aligned} \tag{S17}$$

If more than one symmetry is to be preserved, the constraints due to each of them have to be met simultaneously. Once the T matrices are chosen, an inverse Fourier transform allows to implement the hopping terms in real

space. For example, the nearest neighbor perturbations along x lead to

$$T_{x1}\cos k_x + T_{x2}\sin k_x \to \sum_{x,y}\sum_{\alpha,\beta=1}^{4} c^{\dagger}_{(x,y),\alpha}\left(\frac{T_{x1}-\mathrm{i}T_{x2}}{2}\right)_{\alpha,\beta} c_{(x+1,y),\beta} + h.c., \tag{S18}$$

where the sum over x and y run over the coordinate of unit cells in the entire lattice.

I. Scaling of energies with lattice size

Bound states exponentially penetrate into the bulk of the lattice. Resonances, on the other hand, will have both a 'corner' component, which will exponentially penetrate into the lattice, and a 'bulk' component, which will not. In our scheme for detection of BICs which introduces loss to the bulk but not the corners, the difference in the penetration between BICs and resonances will be manifested by zero imaginary energies for BICs and non-zero imaginary energies for resonances. To rule out the possibility that finite size effects interfere in this differentiation, in this section, we show how the values of the imaginary components of energy vary as the lattice size n increases. This is shown in Fig. S2. In (a), we show the imaginary energies for a lattice with the original Hamiltonian, Eq. 1 of the Main Text, with added perturbations that preserve both C_{4v} and chiral symmetries (implemented as described in Section D). Under these symmetries, corner BICs are protected and thus their imaginary energies are zero (red dots). Bulk states (blue dots), on the other hand, will acquire non-zero imaginary energies due to the losses in the bulk. In (b), perturbations are added to the original lattice, Eq. 1 of the Main Text, which break reflection symmetries. This breaks the mechanism protection of BICs, which the cease to exist as they hybridize with bulk states to form resonances. This is manifested in the fact that the imaginary energies are not zero anymore (purple dots). Notice that the values converge for lattice sizes as low as $n = 16$.

[1] G. H. Wannier, Rev. Mod. Phys. **34**, 645 (1962).
[2] N. Marzari and D. Vanderbilt, Phys. Rev. B **56**, 12847 (1997).
[3] B. Bradlyn, L. Elcoro, J. Cano, M. G. Vergniory, Z. Wang, C. Felser, M. I. Aroyo, and B. A. Bernevig, Nature **547**, 298 EP (2017).
[4] W. A. Benalcazar, T. Li, and T. L. Hughes, Phys. Rev. B **99**, 245151 (2019).

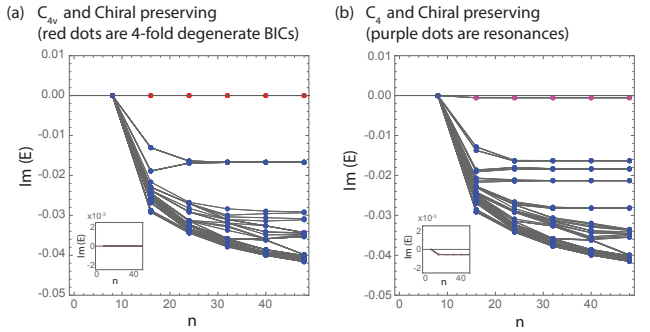

FIG. S2. Imaginary components of energy as a function of lattice size n for a fixed value of system size $n_s = 4$. (a) Lattice preserving both C_{4v} and chiral symmetries. (b) A lattice that breaks C_{4v} down to only C_4 while keeping chiral symmetry. Only in (a) there are BICs (red dots, which are 4-fold degenerate). In (b), as the lattice size increases, the imaginary components of the energies of resonances converge to a non-zero imaginary value (purple dots). The insets are zoomed in versions of (a) and (b) around Im(E)=0.